The 56th International October Conference on Mining and Metallurgy
22-25 October 2025, Bor Lake, Bor, Serbia
www.ioc.tfbor.bg.ac.rs

DOI: 10.5937/IOC25405K *Original scientific paper*

ANALYSIS OF CRACK FORMATION IN AlSi11 ALLOY AUTOMOTIVE RIM

Franjo Kozina[1a], Zdenka Zovko Brodarac[1b], Ivica Buljeta[2a], Natalija Dolić[1c]

[1]Faculty of Metallurgy, University of Zagreb, Aleja narodnih heroja 3, 44000 Sisak, Croatia
[2]Jajce Alloy Wheels d.o.o., Divičani b.b, 70 101 Jajce, Bosnia and Herzegovina
[1a] fkozin@simet.hr, 0000-0002-3219-7771
[1b] zovko@simet.hr, 0000-0002-7892-2633
[1c] ndolic@simet.hr, 0000-0001-5686-6426
[2a] buljeta_ivicay@hoo.com, 0000-0003-0429-5291

Abstract

When manufacturing components with high safety-critical requirements, integrity and reliability must be guaranteed despite the possibility of systemic or random failures. This is complicated by the fact that any of these failures may be caused by random defects inherent in the manufacturing process or operating conditions. The investigation was performed to determine the cause of a permanent random failure in the form of a crack observed during the manufacture and testing of an AlSi11 automotive rim. By correlating the results of chemical composition analysis, thermodynamic calculations, and metallographic analysis, it was found that the crack nucleated on the previously formed shrinkage porosity and propagated across the non-metallic inclusions, the over-modified eutectic (α_{Al} + β_{Si}), Al_5FeSi (β) and $Al_8FeMg_3Si_6$ (π) phases with characteristic morphologies.

***Keywords**: safety-critical requirements, automotive rim, AlSi11 alloy, microstructure, failure*

1. INTRODUCTION

Components with high safety-critical requirements must be designed and developed to guarantee integrity, and reliability throughout the entire life cycle of the product [1]. In the automotive industry, safety is defined as freedom from intolerable risk [2] and includes component malfunction, hazardous situations, the risk of damage or harm and the required risk reduction based on an acceptable level of risk. The severity of the safety requirements assigned to a component or system is defined by the Automotive Safety Integrity Levels (ASIL) and aims to prevent system failures [3]. The identification of hazardous components and the allocation of appropriate ASILs ensures both the intrinsic and functional safety of critical systems without imposing unnecessarily stringent safety-critical requirements on all components [4]. While intrinsic safety ensures that components or systems are designed to minimize the risk of accidents [5], functional safety guarantees that critical systems continue to function even in the event of systemic or random failures. Process-related problems that require changes in design, development, manufacture, operating procedures or documentation are classified as systemic failures. They are usually foreseeable and typically affect multiple units or models of vehicles [4]. Random failures, also known as permanent or transient faults, are caused by random defects innate to the manufacturing process or operating conditions. The main difference between these two types of random failures is that a transient fault is likely to be resolved after a system reset or a change in operating conditions, while a permanent fault is associated with long-term damage that requires physical repair or component replacement [6]. In this study, the permanent random failure in the form of a crack observed during the manufacturing and testing of AlSi11 automotive rim is analyzed. Although the mechanical properties that comply with the standard [7] were achieved, additional tests were performed on the casting to determine the mechanism of crack formation.

2. EXPERIMENTAL

The crack was detected during a radial fatigue test simulating the dynamic load on the wheel when cornering. The crack formed in the hotspot area nucleating on the internal surface of the central cap and propagated towards the inner part of the spoke (Figure 1). As two parts of the rim with different geometries were affected, the investigated area was cut into two parts (Figure 1; positions 1 and 2), with three different positions for testing (Figure 1; positions A, B, C).

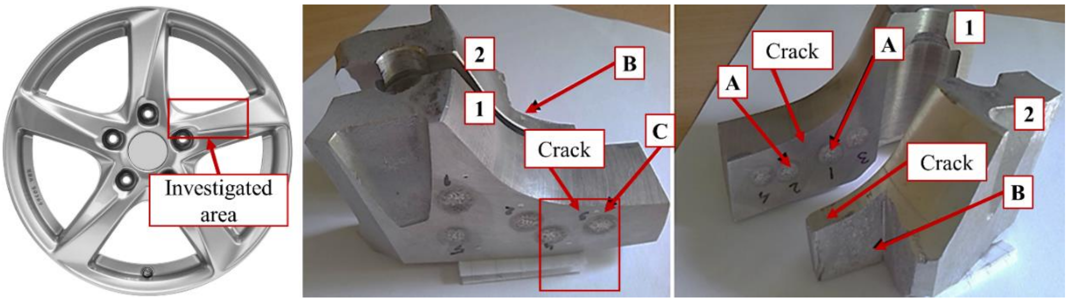

Figure 1. Sampling in the investigated area with the indicated positions for testing (A, B, C)

Since the hotspot is characterized by a lower cooling rate and is the last to solidify, the chemical composition at all three positions (Figure 1; positions A, B, C) was measured spectroscopically using the Thermo Scientific ARL 3460 Metals Analyzer. The analysis of the chemical composition was not only important to verify compliance within the range for EN AC AlSi11 alloy indicated in standard [7] but also served as an input parameter for the calculation of the non-equilibrium solidification sequence. The thermodynamic calculations performed by CALPHAD method using Themo-Calc 2022a TCAL9 technical sheet for aluminum, were based on the classical Scheil-Gulliver model and were calculated in the temperature range from 20.0 °C to 750.0 °C at a default pressure of 100 00.0 Pa for 1.0 g of the melt. The sample for metallographic analysis was cut from the central part of the hotspot (Figure 1, position B), perpendicular to the crack, and prepared using standard metallographic preparation techniques. The sample was then etched for approximately 5 s in a 0.5% aqueous solution of hydrofluoric acid. Light microscopy was performed using an Olympus GX51 inverted metallographic microscope equipped with a DP70 digital camera and AnalySIS Materials ResearchLab software. Electron microscopy was performed using a Tescan, Vega TS 5136 MM scanning electron microscope in combination with a Bruker energy dispersive spectrometer (EDS). The distribution of the elements within the individual microstructural components was determined by point analysis. Based on the research results, the influence of the microstructure on the mechanism of crack formation and propagation will be determined.

3. RESULTS AND DISCUSSION

The chemical composition of the investigated area is shown in Table 1.

Table 1. The mean value and standard deviation of chemical composition measurements at the positions A, B and C (Figure 1)

Chemical composition, wt.%	Si	Fe	Mn	Mg	Sr	Al
Mean value	10.89	0.107	0.002	0.194	0.037	balance
EN AC AlSi11 [7]	10.5-11.8	≤0.15	≤0.05	/	0.025-0.05	balance

The chemical composition corresponds to the values for the EN AC AlSi11 alloy (Table 1) prescribed by standard [7]. The hypoeutectic Si content indicates that the microstructure development will begin with the solidification of the primary α_{Al} dendrites, followed by the eutectic reaction and the solidification of the (α_{Al} + β_{Si}) eutectic phase. The amount of Sr (Table 1) is nominally sufficient to fully modify the (α_{Al} + β_{Si}) eutectic phase and achieve fiber morphology. An unfavorable Mn/Fe of 0.02 along with low cooling rate due to the section thickness can lead to the preferred precipitation of an Al_5FeSi (β) phase with a needle-like morphology.

The invariant reactions of the non-equilibrium solidification sequence are given in Table 2. The solidification sequence begins with the development of the primary α_{Al} dendrites (Table 2, reaction

1) followed by the solidification of the eutectic ($\alpha_{Al} + \beta_{Si}$) (Table 2, reaction 2). Solidification of the Al_2Si_2Sr phase (Table 2, reaction 3) points to the addition of the excess amount of modifier during melt processing causing the over-modification of the eutectic ($\alpha_{Al} + \beta_{Si}$) and negatively affecting the mechanical properties. Due to their coarse, brittle and angular morphology, the Al_5FeSi (β) phase particles (Table 2, reaction 4) enable local stress concentration and formation of microcracks. The negative effect of Al_5FeSi (β) phase is partially reduced by the solidification of $Al_8FeMg_3Si_6$ (π) phase (Table 2, reaction 5) which has a compact morphology and solidifies at the grain boundaries [8]. The non-equilibrium solidification ends with the formation of Mg_2Si phase (Table 2, reaction 6).

Table 2. The invariant reactions of the non-equilibrium solidification sequence

Reaction No.	Reaction	Temperature, °C
1.	LIQUID (L) + FCC_A1 (α_{Al})	588.4
2.	L + DIAMOND_A4 + FCC_A1 ($\alpha_{Al} + \beta_{Si}$)	576.3
3.	L+ AL2SI2SR (Al_2Si_2Sr) + ($\alpha_{Al} + \beta_{Si}$)	573.4
4.	L + Al_2Si_2Sr + ($\alpha_{Al} + \beta_{Si}$) + AL9FE2SI2 (Al_5FeSi (β))	570.7
5.	L+ Al_2Si_2Sr + ($\alpha_{Al} + \beta_{Si}$) + AL18FE2MG7SI10 ($Al_8FeMg_3Si_6$ (π))	558.7
6.	L + Al_2Si_2Sr + ($\alpha_{Al} + \beta_{Si}$) + π-$Al_8FeMg_3Si_6$ + MG2SI_C1 (Mg_2Si)	557.6

The microstructure at the crack root is given in Figures 2 a – 2 c, while the scanning electron images (SEI) of microstructural constituents affecting the crack propagation are shown in Figures 2 d – 2 e. The results of EDS analysis performed on the indicated positions (Figure 2 d to e) are shown in Table 2.

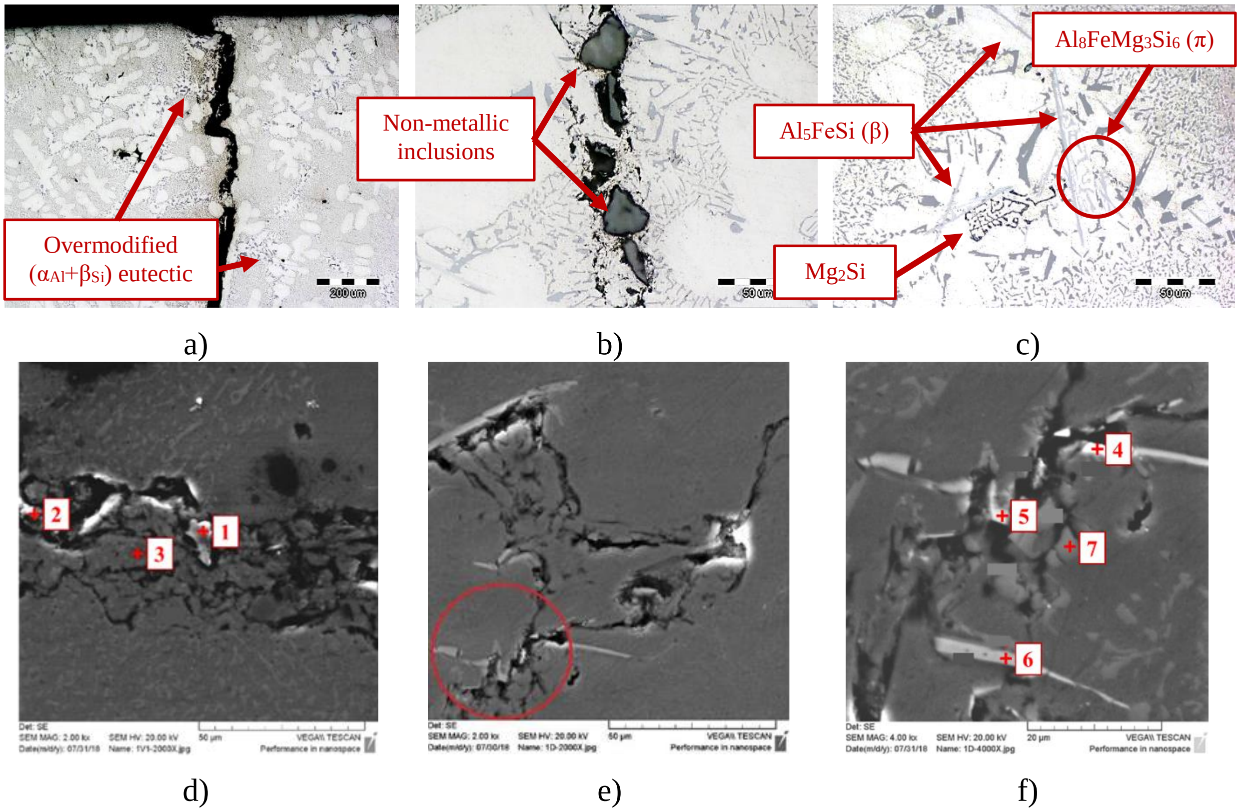

Figure 2. The microstructure at the crack root (a, b, c) and SEI of microstructural constituents affecting the crack propagation (d, e, f)

The microstructure of the sample in the investigated area consists of the primary α_{Al} dendrites and the eutectic ($\alpha_{Al} + \beta_{Si}$) (Figure 2). In addition to the fibrous morphology, an over-modified eutectic ($\alpha_{Al} + \beta_{Si}$) in acicular morphology can be observed at the grain boundaries (Figure 2 a), followed by solidification of $Al_8FeMg_3Si_6$ (π) and Mg_2Si phases. The Al_5FeSi (β) phase is found between the branches of primary α_{Al} dendrites (Figure 2 c). The local stress concentration during the radial fatigue test allowed crack propagation via non-metallic inclusions (Figure 2 b) and intermetallic phases at the grain boundaries (Figure 2 c). The results of SEM and EDS analysis confirmed the involvement of non-metallic inclusions of the alumino-silicate type (Figure 2 d, Table 3, positions 1 and 2), over-modified eutectic (α_{Al} + β_{Si}) (Figure 2 f, Table 3, positions 6), Al_5FeSi (β) and $Al_8FeMg_3Si_6$ (π) phase (Figure 2 f, Table 3, positions 4, 5 and 7).

Table 3. Results of energy dispersive spectroscopy performed at the locations marked on Figure 3

Location	Chemical composition, mass. %				
	Al	Si	Mg	Fe	Mn
1	1.71	96.14	0.74	0.37	0.31
2	4.38	93.60	0.92	0.40	0.31
3	74.11	24.22	1.01	0.30	0.18
4	61.58	13.71	2.21	24.00	2.16
5	60.67	12.95	3.34	22.57	3.43
6	11.92	86.64	0.21	0.36	0.70
7	65.11	12.12	2.36	23.23	0.32

4. CONCLUSION

This research was performed to determine the cause of permanent random failure in the form of a crack that was observed during production and testing of the AlSi11 automotive rim. The chemical composition is in accordance with HRN EN 1706:2021 for investigated alloy. The results of the non-equilibrium solidification sequence indicated development of primary α_{Al} dendrites followed by the solidification of the eutectic (α_{Al} + β_{Si}), Al_2Si_2Sr, Al_5FeSi (β), $Al_8FeMg_3Si_6$ (π) and Mg_2Si phases. The solidification of Al_2Si_2Sr phase pointed to the excess amount of modifier and over-modification of the eutectic (α_{Al} + β_{Si}). The crack nucleation occurred on the grain boundaries and propagated across the non-metallic inclusions, over-modified eutectic (α_{Al} + β_{Si}), Al_5FeSi (β) and Al_8FeMg_3Si6 (π) phase.

ACKNOWLEDGEMENTS

The investigation was performed within the research topic "Design and Characterization of Innovative Engineering Alloys", Code: FPI-124- ZZB funded by University of Zagreb within the Framework of Financial Support of Research and Infrastructural scientific projects: Center for Foundry Technology, Code: KK.01.1.1.02.0020 and VIRTULAB - Integrated Laboratory for Primary and Secondary Raw Materials, Code: KK.01.1.1.02.0022 funded by European Regional Development Fund, Operational Programme Competitiveness and Cohesion 2014 - 2020

REFERENCES

[1] D.J. Thomas, J. Fail. Anal. Prev., 17 (1) (2017) 1–3
[2] ISO 26262-1:2018 Road vehicles — Functional safety (2020).
[3] Y. Gheraibia, S. Kabir, K. Djafri, H. Krimou, J. Fail. Anal. Prev., 18 (3) (2018) 707–720.
[4] P. Okoh, T. Myklebust, Saf. Reliab., 43 (2) (2024) 114–130.
[5] M. V. Kapitonov, Transp. Res. Procedia, 61 (2022) 556–560.
[6] A.C. Bagbaba, F.A. da Silva, M.S. Reorda, S. Hamdioui, M. Jenihhin, C. Sauer, Electron., 11 (3) (2022) 1–26.
[7] HRN EN 1706:2021 Aluminum and aluminum alloys – Castings – Chemical composition and mechanical properties (EN 1706:2020+A1:2021)
[8] H.H. Xi, J.J. Xu, X. Yuan, W.Q. Ming, Z. Zhang, J.H. Chen, Mater. Charact., 199 (2023) 112839